The Astrophysical Journal, 745:72 (6pp), 2012 January 20 doi:10.1088/0004-637X/745/1/72

FAINT HIGH-ENERGY GAMMA-RAY PHOTON EMISSION OF GRB 081006A FROM *FERMI* OBSERVATIONS

WeiKang Zheng[1], Carl W. Akerlof[1], Shashi B. Pandey[1,2], Timothy A. McKay[1], BinBin Zhang[3,4], and Bing Zhang[3]
[1] Department of Physics, University of Michigan, 450 Church Street, Ann Arbor, MI 48109, USA; zwk@umich.edu
[2] Aryabhatta Research Institute of Observational Sciences, Manora Peak, Nainital 263129, India
[3] Department of Physics and Astronomy, University of Nevada, Las Vegas, NV 89154, USA
[4] Department of Astronomy & Astrophysics, Pennsylvania State University, University Park, PA 16802, USA
Received 2011 August 3; accepted 2011 November 18; published 2011 December 29

ABSTRACT

Since the launch of the *Fermi Gamma-ray Space Telescope* on 2008 June 11, the Large Area Telescope (LAT) instrument has firmly detected more than 20 gamma-ray bursts (GRBs) with high-energy photon emission above 100 MeV. Using the matched filter technique, three more GRBs have also shown evidence of correlation with high-energy photon emission as demonstrated by Akerlof et al. In this paper, we present another GRB, GRB 081006A, unambiguously detected by the matched filter technique. This event is associated with more than 13 high-energy photons above 100 MeV. The likelihood analysis code provided by the Fermi Science Support Center generated an independent verification of this detection using a comparison of the test statistics value with similar calculations for random LAT data fields. We have performed detailed temporal and spectral analysis of photons from 8 keV up to 0.8 GeV from the Gamma-ray Burst Monitor and the LAT. The properties of GRB 081006A can be compared to those of the other two long-duration GRBs detected at similar significance, GRB 080825C and GRB 090217A. We find that GRB 081006A is more similar to GRB 080825C with comparable appearances of late high-energy photon emission. As demonstrated previously, there appears to be a surprising dearth of faint LAT GRBs, with only one additional GRB identified in a sample of 74. In this unique period when both *Swift* and *Fermi* are operational, there is some urgency to explore this aspect of GRBs as fully as possible.

Key word: gamma-ray burst: individual (GRB 081006A)

Online-only material: color figures

1. INTRODUCTION

Gamma-ray bursts (GRBs) are extremely luminous explosions in the universe, but most observations are limited to photons below a few MeV. High-energy emission above 100 MeV was only detected a few times by the EGRET instrument (Dingus 1995) and now more recently by *AGILE* (Giuliani et al. 2008). The recently launched *Fermi Gamma-ray Space Telescope* has increased the opportunity to study high-energy radiation from GRBs by providing large apertures and wide fields of view. Two onboard instruments, the Gamma-ray Burst Monitor (GBM; Meegan et al. 2009) and the Large Area Telescope (LAT; Atwood et al. 2009), overlap energy bands to span from 8 keV to above 100 GeV. With other satellites providing more precise localization ability (e.g., *Swift*, Gehrels et al. 2004; *INTEGRAL*, Winkler et al. 2003; *AGILE*, Giuliani et al. 2008), we have a unique opportunity to study the physical mechanisms of GRBs across a very wide dynamic energy range.

The *Fermi*/LAT covers the energy range from below 20 MeV to more than 300 GeV with an effective field of view of ∼2.4 sr (Atwood et al. 2009). The other *Fermi* instrument, the GBM, is sensitive to the 8 keV to 40 MeV range and covers the entire unocculted sky. The GBM identifies GRBs in real time (Meegan et al. 2009) with a rate of ∼250 events per year (Paciesas et al. 2010). During its first 27 month operation, ∼150 GRBs have been detected by the GBM at locations that were simultaneously within the *Fermi*/LAT field of view. However, of these simultaneously observed events,[5] only 20 have been detected at a threshold of more than ∼10 high-energy photons above 100 MeV (Granot 2010), corresponding to a rate of ∼9 GRBs per year.

Using the matched filter technique, the *Fermi* detection threshold was reduced to a level of ∼6 high-energy photons with the concomitant identification of three additional detections as reported by Akerlof et al. (2010, 2011, hereafter A10, A11), namely GRB 080905A, 091208B, and GRB 090228A. In Section 2 we present the first high-energy photon detection of GRB 081006A using this matched filter technique. The detailed observations obtained by the GBM and LAT, including temporal and spectral properties, are described in Section 3. The comparison of GRB 081006A with other two GRBs detected with similar fluences are discussed in Section 4 and summarized in Section 5.

2. DETECTION OF GRB 081006A USING THE MATCHED FILTER TECHNIQUE

Following the method developed by Akerlof et al. in A10 and A11, we apply the matched filter technique to an extended GBM sample by lowering the GBM fluence threshold below the 5 μerg cm^{-2} minimum that defined the GRBs listed in Table 1 of A10. The extended GBM sample consists of either GRBs that have GBM fluences less than 5 μerg cm^{-2} or have no GBM fluence information whatsoever. The remaining criteria are the same as in A10. This new sample of 74 GRBs, listed in Table 1, was searched for high-energy photon emission using the matched filter technique. One GRB, namely GRB 081006A, was revealed with a large matched weight value, $\zeta \sum w_i = 652.460$, more than 26 times larger than any other GRBs in this set. The statistical significance of this detection can be estimated from the cumulative distribution of matched filter

[5] http://fermi.gsfc.nasa.gov/ssc/observations/types/grbs/grb_table/

Table 1
List of 74 GBM-triggered GRBs

GRB	Trigger	R.A. (°)	Decl. (°)	$S_{\rm GBM}$ (μerg cm^{-2})
080805B	080805496	322.70	47.90	...
080822A	080822647	63.60	25.80	...
080824	080824909	122.40	−2.80	2.30
080920	080920268	121.60	8.90	2.40
081006A	081006604	142.00	−67.40	0.71
081006B	081006872	172.20	−61.00	0.73
081107	081107321	51.00	17.10	1.64
081118B	081118876	54.60	−43.30	0.11
081223	081223419	112.50	33.20	1.20
081224	081224887	201.70	75.10	...
081226C	081226156	193.00	26.80	2.32
081226B	081226509	25.50	−47.40	0.61
081229	081229187	172.60	56.90	0.87
081230B	081230871	207.60	−17.30	...
090126B	090126227	189.20	34.10	1.25
090207	090207777	252.70	34.90	4.01
090213	090213236	330.60	−55.00	...
090228B	090228976	357.60	36.70	1.00
090305B	090305052	135.00	74.30	2.70
090306C	090306245	137.00	57.00	0.90
090308B	090308734	21.90	−54.30	3.46
090309B	090309767	174.30	−49.50	4.70
090331	090331681	210.50	3.10	...
090403	090403314	67.10	47.20	...
090413	090413122	266.50	−9.20	...
090429D	090429753	125.21	6.20	1.60
090519B	090519462	105.90	−56.70	1.40
090529B	090529310	231.20	32.20	0.34
090617	090617208	78.89	15.65	0.47
090623B	090623913	41.70	1.80	...
090625A	090625234	20.29	−6.43	0.88
090629	090629543	8.48	17.67	...
090701	090701225	114.69	−42.07	0.45
090703	090703329	0.77	9.68	0.68
090706	090706283	205.07	−47.07	1.50
090717B	090717111	246.95	22.97	0.48
090718A	090718720	243.76	−6.68	...
090726B	090726218	240.45	36.75	...
090807B	090807832	326.90	7.23	1.02
090815C	090815946	251.26	52.93	...
090819	090819607	49.08	−67.12	...
090820B	090820509	318.26	−18.58	1.16
090826	090826068	140.62	−0.11	1.26
090907B	090907808	81.06	20.50	...
090917	090917661	230.34	−11.69	...
091002	091002685	41.92	−14.01	...
091017B	091017985	214.40	−64.74	...
091024B	091024380	339.25	56.88	...
091107	091107635	182.35	38.94	...
091109C	091109895	247.72	42.31	...
091115	091115177	307.76	71.46	...
091207A	091207333	12.67	−50.19	...
091219	091219462	294.49	71.91	...
091223A	091223191	203.23	76.35	...
091231B	091231206	199.36	−60.70	...
100101B	100101988	70.66	18.69	...
100201A	100201588	133.10	−37.29	...
100212B	100212550	134.27	32.22	...
100218A	100218194	206.64	−11.94	2.58
100301A	100301068	110.14	−15.68	...
100313B	100313509	186.37	11.72	...
100315A	100315361	208.90	30.14	...
100325B	100325246	209.14	−79.10	...
100330B	100330856	326.38	−6.97	...
100401A	100401297	281.85	−27.83	2.39

Table 1
(Continued)

GRB	Trigger	R.A. (°)	Decl. (°)	$S_{\rm GBM}$ (μerg cm^{-2})
100417A	100417166	261.31	50.38	...
100427A	100427356	89.17	−3.46	3.01
100429A	100429999	89.09	−69.96	...
100516A	100516014	117.32	55.14	...
100517B	100517132	40.63	−44.32	...
100605A	100605774	273.43	−67.60	...
100608A	100608382	30.54	20.45	...
100620A	100620119	80.10	−51.68	...
100625B	100625891	338.26	20.29	...

Table 2
List of High-energy Photons for GRB 081006A

i[a]	t[b]	θ[c] (°)	E[d] (MeV)	c[e]	w_i[f]
1	1.948	1.136	210.759	3	157.796
2	6.384	1.253	130.083	3	138.073
3	2.970	1.054	645.476	3	118.829
4	13.251	0.809	787.895	3	59.160
5	11.438	1.298	113.833	3	55.808
6	2.048	0.372	283.650	2	51.225
7	2.268	0.844	115.327	3	47.475
8	6.806	1.348	148.296	2	27.328
9	19.615	1.546	375.440	1	0.570
10	3.076	1.762	567.849	1	0.354
11	32.331	8.859	121.218	2	0.121
12	26.478	0.132	773.543	3	0.094[g]
13	42.549	5.612	150.876	1	0.002
GRB 081006A	$\zeta = 0.99334$		$\zeta \sum w_i = 652.460$		

Notes.
[a] Photon ID number.
[b] Time after the trigger.
[c] Distance to the new estimated GRB location.
[d] Energy of each photon.
[e] Photon class.
[f] Weight of each photon.
[g] Indicates diminished w_E for highest energy triplet cluster photon.

weights for a large sample of otherwise similar LAT fields. As shown in Figure 4, after including the GBM-triggered sample size of 74, the probability of such an event arising from random background photons is significantly less than 0.4%. A more detailed discussion is provided in Section 3.2

The triplet cluster finder associated with the matched filter technique estimates the location of GRB 081006A to be R.A. = 134.°4 and decl. = −61.°8 (J2000.0) with an uncertainty of ∼0.°5. Thirteen high-energy photons are spatially clustered in the nominal GRB 081006A direction. As shown in Table 2, 11 of these photons lie within a 2° radius. Figure 1 shows the LAT photon sky map of GRB 081006A. Our estimated direction (filled blue dot) is 6.°6 away from the GBM determination (center of the map) which has a 1σ uncertainty of 4.°5 with an additional systematic uncertainty of the order of 2.°5 (van der Horst 2008), thus demonstrating consistency at the 1σ level. We note that GRB 081006A occurred ∼120 s before the LAT ceased to take data as the satellite moved closer to the South Atlantic Anomaly (SAA). This must be accompanied by an increased photon background rate, but over the whole LAT field before and after the GRB trigger we find no significant rate change that

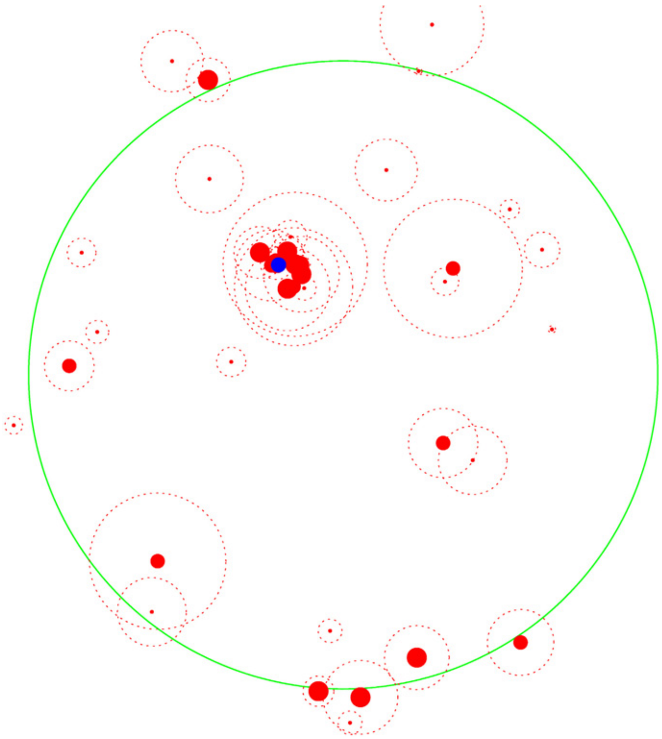

Figure 1. LAT high-energy photons sky map for GRB 081006A. The diameter of each dot is proportional to its statistical weight. Thus, the largest diameters represent event class 3, etc. The dotted circles around each point indicate the $1-\sigma$ errors. The figure is centered on the nominal coordinates furnished by the GBM; the blue dot on the lower left shows the GRB coordinates computed by the cluster algorithm described in the text. The large green circle depicts the boundaries of the 16°.0 radius cone that defines the fiducial boundaries for the cluster search. The plot axes are aligned so that north is up and east is to the right.

(A color version of this figure is available in the online journal.)

would create a spurious event that could mimic the signature of GRB 081006A.

3. *FERMI* GBM AND LAT OBSERVATIONS

3.1. GBM Observations

At 14:29:34 UT on 2008 October 6, the *Fermi* GBM triggered and located GRB 081006A (trigger 244996175/081006604; van der Horst 2008). Using the GBM trigger data, the on-ground calculated location was R.A. = 142°.4, decl. = −67°.4 (J2000) with an uncertainty of 4°.5 (1σ containment, statistical only). The GRB T_{90} is ∼7 s long (van der Horst 2008), clearly detected by NaI detector numbers 0 and 3. The bismuth germanate (BGO) detector located on the same side, B0, also detected the increased flux.

Figure 2 shows the light curves obtained by the GBM and LAT. The upper plot is the background-subtracted light curve for the two NaI detectors, N0 + N3, in the 8–800 keV energy range. The counts were binned in 0.5 s intervals to provide a good visual representation of the intensity behavior. The middle plot is the background-subtracted light curve for the BGO (B0) detector in 280 keV to 4 MeV energy range with the same time binning. The GBM data show a single peak concentrated in the first 2 s after the trigger. The lower plot is the light curve for the LAT detector above 100 MeV within an angle of 12° with respect to the nominal GBM direction described above.

3.2. LAT Observations

The boresight angle of GRB 081006A with respect to the LAT was 16° at the time of the trigger. The LAT did not slew to the burst direction but remained in normal observation mode, taking data for ∼120 s before entering the SAA. GRB 081006A was not reported by the LAT team but we have shown that it is unambiguously identified by the matched filter technique. With at least 13 high-energy photons detected, it is bright enough to allow a likelihood analysis using the standard Science Tools software package[6] provided by the Fermi Science Support Center (FSSC).

The *gtlike* tool, part of the standard Science Tools software package, generates the test statistic TS = $2\Delta\log(\text{likelihood})$ to compare models with and without an assumed source. The TS value associated with each source is a measure of the source significance or equivalently the probability that such an excess can be obtained from background fluctuations alone. A TS value of 25 corresponds to a 4.6σ significance, approximately the square root of TS (Abdo et al. 2010).

The first step to perform a likelihood analysis with the *gtlike* tool is the selection of the LAT events belonging to the TRANSIENT class, reconstructed under the current instrument response functions: Pass6_V3. Following FSSC suggestions, the selected energy range spanned from 100 MeV to 100 GeV. The data below 100 MeV cause large uncertainties due to rapidly changing effective area with energy as well as ambiguity in the instrument response. We also set the maximum zenith angle value of 105° as suggested in the *Fermi* data processing "Cicerone."[7] Finally, the time range for GRB data was set to be 0–50 s after the burst trigger time (T0), almost the same as described by Akerlof et al. (A10; A11).

The localization of GRB 081006A was also obtained from the TS map. The best-fit position from the *gtfindsrc* procedure is R.A. = 135°.53 and decl. = −61°.65 (J2000). Figure 3 shows the error contours around the fitted position with 68%, 90%, and 99% statistical error radii of 0°.4, 0°.6, and 0°.9, respectively. This position is 0°.55 from the location derived from the matched filter technique. Thus, the locations derived from the two methods are consistent to within 1σ error.

The likelihood analysis indicates a detection with a TS value of 45 assuming an isotropic background model. Considering that GRB 081006A is close to the Galactic plane ($b \sim -0°.9$), we must be careful that the high-energy photon background does not have a local hot spot. However, a counts map with data taken three weeks prior to the burst demonstrated that the GRB position is safely >10° away from the bright region near the Galactic plane. We also estimated the count rate using the pre-burst data and re-scaled to the 50 s time range with TRANSIENT class events. Both these methods show that the background is not more than three photons in the 0–50 s time range. The TS detection value of 45 for GRB 081006A is close to the significance of GRB 080825C (Abdo et al. 2009d), GRB 081024B (Abdo et al. 2011), and GRB 090217A (Ackermann et al. 2010).

In order to estimate the probability of such an occurrence by chance alone, we performed identical searches using the likelihood analysis method on 16,088 random LAT fields that were selected similarly to the procedure described in A10. Considering that the likelihood analysis is extremely time consuming, about 15 minutes on a PC, we only applied the

[6] http://fermi.gsfc.nasa.gov/ssc/data/analysis/

[7] http://fermi.gsfc.nasa.gov/ssc/data/analysis/documentation/Cicerone/

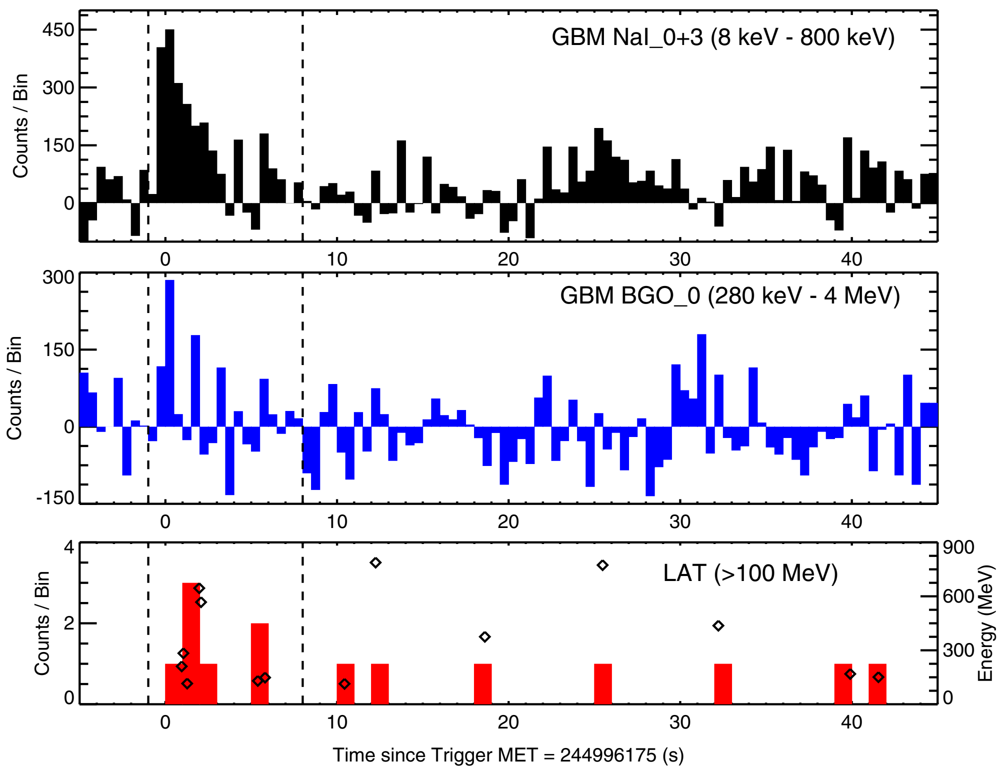

Figure 2. GBM and LAT light curves for GRB 081006A, in the order of increasing energy from top to bottom. The upper plot is the background-subtracted sum of counts in the two NaI detectors, (N0 + N3), in the 8–800 keV energy range with a 0.5 s bin size. The middle plot is the background-subtracted counts in the BGO (B0) detector in the 280 keV to 4 MeV energy range with a 0.5 s bin size. The lower plot shows the number of LAT events which passed the TRANSIENT event selection above 100 MeV, bin step is 1 s. The open diamonds represent the energy for each photon.

(A color version of this figure is available in the online journal.)

likelihood analysis to the 2192 random fields (out of the 16,088) that contained more than three photons of class 2 or 3 within a 16° radius region. If there are fewer than three class 2 or 3 photons within the region, it is almost impossible to detect a reliable GRB signal. Figure 4 (upper panel) shows the cumulative distributions of the TS value for these 2192 random fields and the 27 (out of the 74) GRB fields that pass the same criteria. A Kolmogorov–Smirnov test indicates that the two distributions are consistent if we exclude the outlier, GRB 081006A. The random fields analysis shows that none has a TS value exceeding the candidate event, GRB 081006A. The bottom panel of Figure 4 shows the cumulative distributions of the matched weight value ($\zeta \sum w_i$) derived from the statistical technique described in A10.

In view of the heavy computational demands of the maximum likelihood method and the meager number of GRBs associated with high-energy LAT photons, we decided to make some specific comparisons with the matched weight technique which is at least a thousand times faster to compute. The distributions shown in Figure 4 indicate that the number of random fields that need to be examined to find a single event at the significance level of GRB 081006A is computationally daunting. Without embarking on such a brutal course the most conservative comparison of the statistical power of the two methods is obtained by noting that the random probability of obtaining a TS value greater than 45 is less than $0.0123 = 27/2192$ and the random probability of obtaining a matched weight value greater than 652 is less than $0.0043 = 74/17{,}200$. Thus, the matched filter technique is at least three times more effective in rejecting background. A more realistic estimate can be obtained by

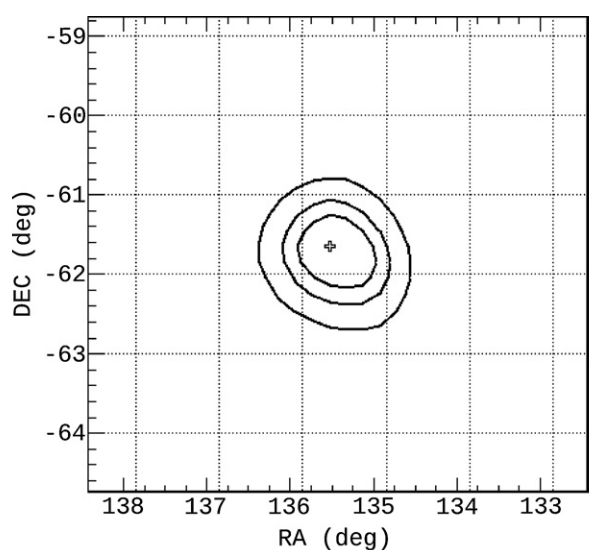

Figure 3. LAT localization for GRB 081006A with best-fit position R.A. = 135°.53 and decl. = −61°.65 (J2000). The contours around the estimated position show a 68%, 90%, and 99% statistical error radius of 0°.4, 0°.6, and 0°.9, respectively.

assuming exponential decreases of the cumulative distributions with the relevant parameters. These estimated trends are shown by the cyan lines in the two graphs. This would suggest that the matched filter rejects background for similar events at a level at least 50 times better than the maximum likelihood approach. Thus, the false positive probability for this GRB identification is of the order of 10^{-5}.

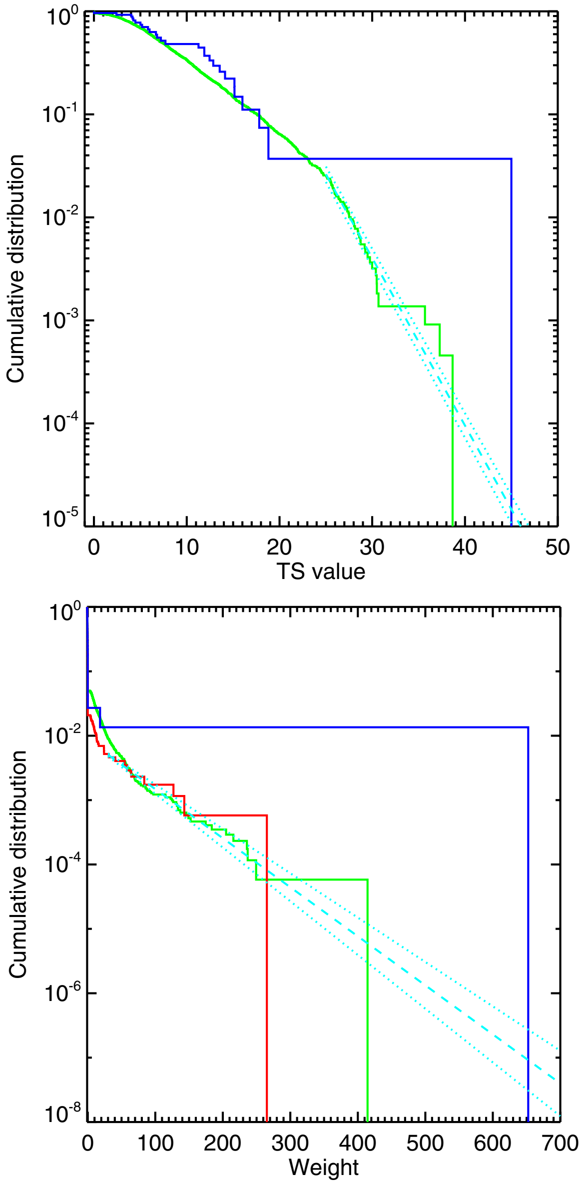

Figure 4. Upper panel: complements of the cumulative distributions for TS values of 27 GBM GRBs (blue) and 2192 similar fields obtained at random times (green). Bottom panel: the cumulative distributions for the matched weight values ($\zeta \sum w_i$) of 74 GBM GRBs (blue), 1731 random fields obtained nearly simultaneously with the GBM data (red), and 17,200 random fields obtained at random times (green). The dashed lines (cyan) in the two panels are extrapolations based on fits described in the text. (The dotted lines indicate estimated statistical uncertainties.)

With the localization obtained from the matched filter technique, the likelihood analysis confirmed the identification of faint LAT GRB 081006A. In several ways, these two methods are complimentary. The matched filter is computationally efficient for identifying weak signals with predetermined characteristics while the maximum likelihood method works best when the combinatorial background is relatively easy to estimate. The overall success of this approach is illustrated by GRB 081006A as well as the discoveries reported in previous papers.

3.3. *Joint Spectral Fitting with GBM and LAT Data*

Joint spectral fitting with the GBM and LAT data was performed for the time range, −1 s to 8 s, after the trigger. Due to the faintness of the burst, time-resolved spectral fitting is not appropriate. RMFIT (version 3.3) software was used for spectral fitting with binned GBM time-tagged event data. The LAT data are re-binned to match the format required by RMFIT.

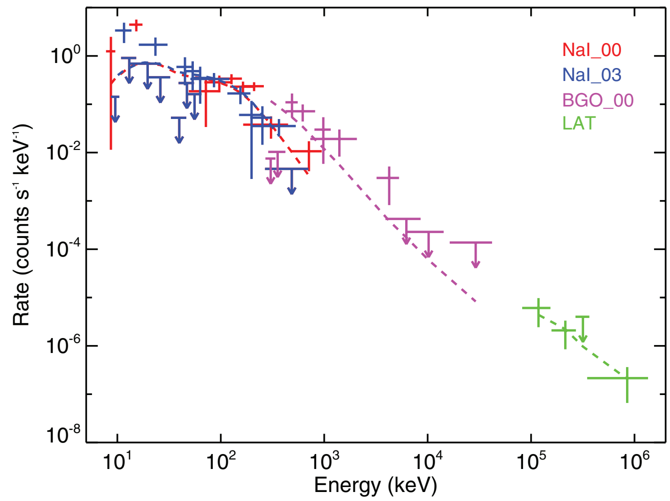

Figure 5. Spectral distribution of time-integrated (−1 s to 8 s) GRB 081006A photons obtained from the GBM and LAT data. The spectrum is well fit by a Band function model spanning ∼5 decades of energy. The data from each instrument are indicated by color: red = NaI 0, blue = NaI 3, pink = BGO 0, and green = LAT. The dashed lines depict the fit obtained with the Band function model convolved with the four different instrument response functions.

Figure 5 shows the simultaneous fitting of the time-averaged count spectra from the GBM and LAT data. The Band function model (Band et al. 1993) fit to the GBM and LAT data gives a reasonably good fit with amplitude $A = 2.1^{+0.6}_{-0.4}\ 10^{-3}$ (photons cm^{-2} s^{-1} keV^{-1}), $E_p = 817.0^{+827}_{-340}$ (keV), $\alpha = 0.78^{+0.35}_{-0.24}$, and $\beta = 2.28\ ^{+0.10}_{-0.14}$ (χ^2/dof = 464/379). The corresponding energy flux is $(2.18 \pm 0.22) \times 10^{-7}$ erg cm^{-2} s^{-1} in the 10 keV to 1 MeV range and $(6.06 \pm 0.61) \times 10^{-7}$ erg cm^{-2} s^{-1} in the 10 keV to 1 GeV range. E_p of GRB 081006A is not well constrained, as already noticed by van der Horst (2008), but the Band function model fitting is clearly better than a single power-law model or a power law with exponential cutoff model. Given that some GRBs have more complex spectral behavior than described by the Band function (e.g., Zhang et al. 2011), we also tried a two-component Band function plus power law, and also the Band function plus thermal component, but the fit was not improved.

4. DISCUSSION

GRB 081006A is detected with a fluence similar to three other GRBs, namely GRB 080825C, 081024B, and 090217A. Among these events, GRB 081024B is a short-duration burst while GRB 080825C and GRB 090217A are long duration. We thus compare the properties of GRB 081006A, also a long-duration burst, with GRB 080825C and GRB 090217A.

The overall spectral features of GRB 081006A are quite similar to those of GRB 080825C and 090217A: they can be fitted by the Band function model over five-decade energy range from 8 keV to 800 MeV. No cutoff feature in the LAT energy range is detected. This suggests that a single emission mechanism is responsible for the broadband emission of both GBM and LAT, e.g., synchrotron or jitter emission from the internal shock (Medvedev 2000).

The delayed onset of high-energy LAT emission (>100 MeV), observed for many other LAT-detected GRBs (e.g., GRB 080825C, Abdo et al. 2009d; GRB 080916C, Abdo et al.

2009c; GRB 090510, Abdo et al. 2009b; GRB 090902B, Abdo et al. 2009a), also shows a hint in GRB 081006A. The initial peak of LAT high-energy photons with GRB 081006A, though correlated with the GBM peak, is delayed for about 2 s after the low-energy GBM trigger. The delayed emission of high-energy photons from GRB 081006A is not as pronounced, as found for GRB 080825C. In the later case, the onset of LAT emission is occurs at about 3 s and the first LAT peak is coincident with the second GBM peak (Abdo et al. 2009d), but it is different from GRB 090217A for which there was no perceptible delay (Ackermann et al. 2010).

Many GRBs (e.g., GRB 080825C, Abdo et al. 2009d; GRB 080916C, Abdo et al. 2009c; GRB 090510, Abdo et al. 2009b; GRB 090902B, Abdo et al. 2009a) also have long-lived high-energy photon emission detected by the LAT even hours after the burst. The high-energy photon emission of GRB 081006A clearly lasts longer (∼40 s in LAT data) than the low-energy emission (GBM; $T_{90} \sim 7$ s). The two highest energy photons, both with $E \sim 780$ MeV, are detected at 13.25 s and 26.5 s after the trigger as shown in Table 2. This is also similar to GRB 080825C for which the LAT emission lasted slightly longer (up to $T_0 + 35$ s) than for the GBM ($T_{90} = 27$ s). GRB 090217A does not show such longer higher energy emission.

5. SUMMARY

We have demonstrated the association of GRB 081006A with high-energy photon emission by applying the matched filter technique to the *Fermi*/LAT data. The false positive probability is definitely less than 4×10^{-3} and probably much smaller. This event is found to be correlated with at least 13 high-energy photons detected by the LAT instrument. A maximum likelihood analysis reveals a similar confidence level with a TS value of 45. Comparing the temporal and spectral properties with the other two long-duration GRBs with similar fluences, GRB 080825C and 090217A, we find GRB 081006A is closer to GRB 080825C. The delay and long emission duration for high-energy photons are seen in GRB 081006A, similar to GRB 080825C, but not with GRB 090217A. These properties can be examined in more detail as the *Fermi* mission continues to obtain a larger sample of GRBs, especially faint ones such as GRB 081006A, 080825C, and 090217A. As demonstrated here, the matched filter technique is considerably more sensitive than the maximum likelihood analysis to find these fainter events. In the particular case of GRB 081006A, the background rejection is approximately 50 times better, making it a far better search tool for these rare events. As we have shown with several original identifications of faint LAT GRBs, the two methods are best employed sequentially to first find the events and, second, to determine the event characteristics. In this unique period when both *Swift* and *Fermi* are operational, there is some urgency to explore the surprising dearth of faint LAT GRBs as fully as possible.

We thank Lin Lin at NAOC/UAH for valuable suggestions about the GBM data analysis. This research is supported by the NASA grant NNX08AV63G and the NSF grant PHY-0801007.

REFERENCES

Abdo, A. A., Ackermann, M., Ajello, M., et al. 2009a, ApJ, 706, L138
Abdo, A. A., Ackermann, M., Ajello, M., et al. 2009b, Nature, 462, 331
Abdo, A. A., Ackermann, M., Ajello, M., et al. 2010, ApJS, 183, 46
Abdo, A. A., Ackermann, M., Ajello, M., et al. 2011, ApJ, in press (arXiv:1002.3205)
Abdo, A. A., Ackermann, M., Arimoto, M., et al. 2009c, Science, 323, 1688
Abdo, A. A., Ackermann, M., Asano, K., et al. 2009d, ApJ, 707, 580
Ackermann, M., Ajello, M., Baldini, L., et al. 2010, ApJ, 717, L127
Akerlof, C., Zheng, W., Pandey, S. B., & McKay, T. A. 2010, ApJ, 725, L15 (A10)
Akerlof, C., Zheng, W., Pandey, S. B., & McKay, T. A. 2011, ApJ, 726, 22 (A11)
Atwood, W. B., Abdo, A. A., Ackermann, M., et al. 2009, ApJ, 697, 1071
Band, D., Matteson, J., Ford, L., et al. 1993, ApJ, 413, 281
Dingus, B. L. 1995, Ap&SS, 231, 187
Gehrels, N., Chincarini, G., Giommi, P., et al. 2004, ApJ, 611, 1005
Giuliani, A., Mereghetti, S., Fornari, F., et al. 2008, A&A, 491, 25
Granot, J. 2010, in The Shocking Universe: Gamma-ray Bursts and High Energy Shock Phenomena, Venice, September 14–18, 2009 (Bologna: Italian Physical Society) (arXiv:1003.2452)
Medvedev, M. V. 2000, ApJ, 540, 704
Meegan, C., Lichti, G., Bhat, P. N., et al. 2009, ApJ, 702, 791
Paciesas, W., et al. 2010, BAAS, 41, 669
van der Horst, A. J. 2008, GCN Circ., 8341, 1
Winkler, C., Courvoisier, T. J.-L., Di Cocco, G., et al. 2003, A&A, 411, L1
Zhang, B.-B., Zhang, B., Liang, E., et al. 2011, ApJ, 730, 141